Highly-efficient electrochemical label-free immunosensor for the detection of ochratoxin A in coffee samples

Kwanele Kunene, Matthieu Weber, Myalowenkosi Sabela, Damien Voiry, Suvardhan Kanchi, Krishna Bisetty, Mikhael Bechelany

Highly-efficient electrochemical label-free immunosensor for the detection of ochratoxin A in coffee samples

Kwanele Kunene[a,b], Matthieu Weber[a], Myalowenkosi Sabela[b], Damien Voiry[a], Suvardhan Kanchi[b] , Krishna Bisetty[b,*] and Mikhael Bechelany[a,*]

[a]*Institut Européen des Membranes, UMR 5635 ENSCM-UM-CNRS Université Montpellier, Place Eugene Bataillon, F-34095 Montpellier Cedex 5, France*

[b]*Department of Chemistry, Durban University of Technology, P.O. Box 1334, Durban 4000, South Africa*

[†]Corresponding authors. mikhael.bechelany@umontpellier.fr (M. Bechelany), bisettyk@dut.ac.za (K. Bisetty)

Abstract

Ochratoxin A (OTA) is among the most important mycotoxins classified as potential risks to human health and food safety. In this work, a novel label-free electrochemical immunosensor has been proposed for the quantitative detection of OTA, based on a two-step strategy for the fabrication of the immunosensor. This involved coating of a carbon felt (CF) electrode with palladium nanoparticles (PdNPs) using atomic layer deposition (ALD), followed by the grafting of the anti-OTA antibodies onto the nanocomposite structure using a carbodiimide functional group via a cross linkage route. Cyclic voltammetry (CV) and electrochemical impedance spectroscopy (EIS) have been employed for the characterization of the immunosensor properties. The fabricated BSA/anti-OTA/PdNPs/CF immunosensor showed outstanding electrochemical performance towards the detection of OTA in spiked coffee samples. At the optimal working conditions, the linear detection range of the developed immunosensor was from 0.5-20 ng mL^{-1} (R^2 = 0.996) with a low detection limit of 0.096 ng mL^{-1}, making it applicable to the screening of OTA in food products. In addition, the sensor was highly selective to OTA in the presence of interfering compounds and revealed stability

of up to three weeks, opening up prospects for the molecular sensing community and paving a new route for quality control in the food industry.

Keywords: Electrochemical immunosensor, Ochratoxin A, Carbon felts electrode, Palladium nanoparticles, Atomic Layer Deposition

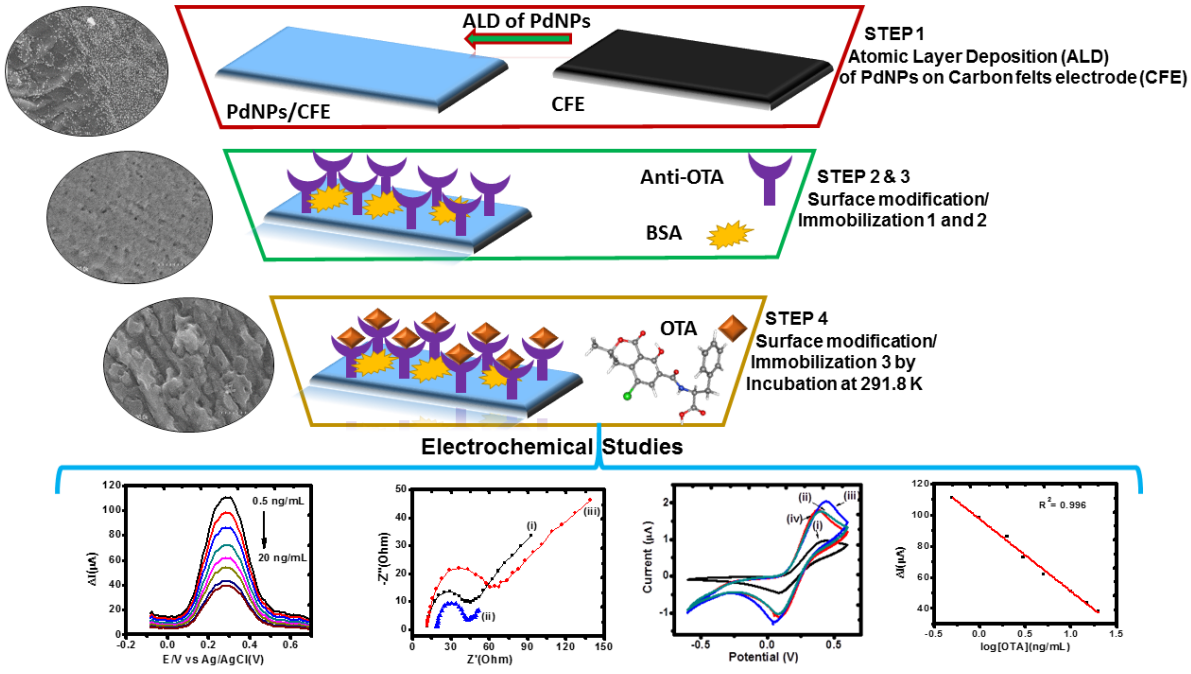

1. Introduction

Ochratoxin A (OTA) is one of the secondary fungal metabolite that occurs naturally and is present in many food products and produced by a number of fungal species such as *Aspergillus ochraceus* and *Penicillium verrucosum* [1]. OTA is primarily found in food commodities such as cereals, coffee beans, and wine [2-4]. Different studies reported that OTA is among the most abundant and toxic mycotoxins due to their high hepatotoxic, nephrotoxic, teratogenic, and mutagenic effects to most mammalian species [5, 6]. They are suspected of being one of the main cause of immuno suppression and immuno toxicity [7],

therefore, policies have been implemented in order to limit their toxicity in food products. For example, the European Union (E.U.) has established maximum permitted limits for OTA depending on the food products: 5.0 µg kg^{-1} for unprocessed cereals, 10.0 µg kg^{-1} for dried fruits, 15.0 µg kg^{-1} for spices, 2.0 mg mL^{-1} for all types of wines and 10 ng mL^{-1} for coffee beans [2, 8, 9]. Consequently, the development of suitable analytical techniques to efficiently monitor OTA concentrations in food products has become crucial.

Conventional analytical techniques for the determination of OTA involves thin layer chromatography (TLC) [10], gas chromatography (GC) [11], liquid chromatography mass spectrometry (LC/MS) [12], photoluminescence [13, 14], enzyme-linked immunosorbent assay (ELISA) [15] ultra high performance chromatography-tandem mass spectrometry (UHPLC-MS/MS) [16] and high performance liquid chromatography (HPLC) [17, 18]. However, these techniques require extensive sample preparation, highly trained personnel and are time consuming and costly. Thus, alternative methods offering high sensitivity, cost-effectiveness, fast and portable detection such as fluorescence [19], chemiluminescence [20] or electrochemistry [21, 22] have been developed. Previous reports have shown that electrochemistry techniques are fast and sensitive (in the ng mL^{-1} range), but with limited selectivity. For this reason, a steady shift towards aptasensors or biosensor techniques has been implemented, opening new promising paths for analysts. [19, 23].

Previously, various nanomaterials have been used for the development of efficient electrochemical immunosensors for OTA detection in different food products [24, 25]. As reported by Taghdisi and co-workers [26], the use of nanoparticles in electrochemical sensing devices is an extremely promising prospect, since they are biocompatible and able to retain the biological activity upon absorption, to enable the direct electron transfer through the conducting tunnels and the enhancement of immobilization of antibodies [27, 28]. Bonel and

co-workers developed indirect and competitive electrochemical immunosensors for the detection of OTA in wheat, using screen-printed carbon electrode (SPCE) on which OTA were conjugated to bovine serum albumin (OTA-BSA) and gold nanoparticles (OTA-BSA-AuNPs). The immunosensor showed a linear detection range (LDR) of 0.3 to 8.5 ng mL^{-1}, with a limit of detection (LOD) of 0.86 ng mL^{-1} [25]. Another biosensor was reported by Rivas and co-workers where (SPCE) modified with polythionine (PTH) and iridium oxide nanoparticles (IrO_2 NPs) were used for the detection of OTA in wine samples. The label-free aptasensor showed the LDR of 0.004 and 40 ng mL^{-1}, and found the lowest LOD reported so far for label-free impedimetric detection of OTA (14 pM) [24]. Karczmarczyk and co-workers developed a sensitive indirect competitive assay quartz crystal microbalance with dissipation monitoring (QCM-D) sensor for detection of OTA in red wine. They amplified the QCM-D signal by combining the secondary antibodies with gold nanoparticles (AuNPs), and found a LODs of 0.16 ng mL^{-1} in the LDR of 0.2–40 ng mL^{-1} [4]. Zhang and co-workers represents the amplified voltammetric immunoassay for OTA in red wine. They achieved this by enclosing platinum on gold cores (AuPtNP) and functionalized it with monoclonal antibodies. The system presented a LDR of 0.2 to 5×10^3 pg mL^{-1} of OTA, with a lower LOD of 0.75 pg mL^{-1} [29]. However, the above reported immunosensors for OTA detection were based on complex methods for synthesis of nanomaterials and were often fabricated using multiple routes. Thus, novel and easier routes enabling the fabrication of immunosensing devices are highly desired.

Atomic layer deposition (ALD) is a novel promising strategy for the direct growth of both thin films and nanoparticles with controllable dimensions at the nanometer scale [30, 31]. This vapor phase technology is based on the sequential use of self-limiting chemical reactions, enabling the synthesis of high quality inorganic nanomaterials in challenging substrates, with

a precise control over their thickness. These benefits permitted this technique to become an essential tool for the deposition of nanomaterials for a myriad of applications, such as microelectronics [32], but also catalysis [33], membranes [34] and biosensing [35].

In the present work, we report a novel PdNPs/carbon nanocomposite based immunosensor for the efficient detection of OTA in coffee samples, using a two-step strategy for the fabrication of the immunosensor. Firstly, ALD was employed to coat CF substrates with highly dispersed palladium nanoparticles (PdNPs), and the anti-OTA were then grafted to the composite structure using a carbodiimide cross linkage route. Next, the composite structures were characterized in terms of physical and chemical properties, using scanning electron microscopy (SEM), transmission electron microscopy (TEM) and attenuated total reflectance (ATR). The immunosensor was then tested for the detection of OTA in spiked coffee samples using differential pulse voltammetry (DPV) and assessed on LODs, reproducibility and selectivity.

2. Experimental section

2.1 Materials and methods

The carbon felt (CF) AvCarb® MGL190 was purchased from Johnson Matthey Co., Germany. Modified carbon felt electrode (CFE) were used as the working electrode, graphite rode as the counter electrode and Ag/AgCl as the reference electrode. The dimensions of the working electrode supports were 3.5 cm length, 0.7 cm width, and 0.3 cm thickness. *N*-(3-dimethylaminopropyl)-N'-ethycabordiimide (EDC)(CAS Number 1892-57-5, purity 97.0%), *N*-hydroxysuccinimide (NHS)(CAS Number 6066-82-6, purity 98.0%), potassium ferricyanide ($K_3Fe(CN)_6$ (CAS Number 13746-66-2, purity 99.0%), potassium ferrocyanide ($K_4Fe(CN)_6$ (CAS Number 14459-95-1, purity 98.5-102.0%), potassium hydrogen phosphate

(K_2HPO_4) (CAS Number 7758-11-4, purity 98.0%), potassium dihydrogen phosphate (KH_2PO_4) (CAS Number 7778-77-0, purity 99.0%), phosphate buffered saline tablet (PBS) (CAS Number 0000000000), palladium (II) hexafluoroacetylacetonate ($Pd(hfac)_2$ (CAS Number 64916-48-9, purity 99.0%), OTA standard solution (OTA), 1 mg mL^{-1} in DMSO (CAS Number 303-47-9, purity 98.0%), formaldehyde solution (CH_2O) (CAS Number 50-00-0, ACS reagent, 37 wt. % in H_2O, contains 10-15% Methanol as stabilizer) and Bovine serum albumin solution (BSA) (CAS Number 9048-46-8, purity 98.0%) were purchased from Sigma-Aldrich, France. Monoclonal antibody anti-ochratoxin A (anti-OTA) (Catalog #: ICP9948, 250 µg mL^{-1} in PBS 50% glycerol) was obtained from Immune Chem Pharmaceutical Incl (Canada). Nescafe (NES, Vevey, Switzerland) obtained from a local supermarket. Double distilled water was used for all experiments.

2.2 Apparatus

The modified CF electrodes were characterized by scanning electron microscopy (SEM, Hitachi S-4800). The contact angle (CA) measurements of PdNPs/CF and BSA/anti-OTA/PdNPs/CF electrodes were conducted on a homemade contact angle setup. During measurement, a drop of deionized water was deposited over the electrode surface and the angle of the liquid surface with contact surface was observed at the solid-liquid interface. attenuated total reflectance (ATR) spectra were collected using iS50 ATR Thermo scientific spectrophotometer. Electrochemical measurements such as cyclic voltammetry (CV), differential pulsed voltammetry (DPV) and electrochemical impedance spectroscopy (EIS) were performed at room temperature (~ 25.0 °C) using a SP-150 EC-LAB Electrochemistry chemical workstation (VSP Potentiostat from BioLogic Science Instruments, France). Transmission electron microscopy (TEM) was performed using a JEOL 2200FS (200 kV).

2.3 Synthesis of palladium nanoparticles (PdNPs) by Atomic Layer Deposition (ALD)

In this work, the highly dispersed PdNPs were synthesized by applying 200 ALD cycles in a low-pressure hot-wall (home-built) ALD reactor. ALD was achieved using sequential exposures of $Pd(hfac)_2$ and formalin separated by Argon purges. If not specified otherwise, the ALD cycle consisted of 5 s pulse of $Pd(hfac)_2$, 15 s of gas exposure, 10 s of purge with Argon followed by 1 s pulse of formalin, 15 s of exposure and finally 60 s purge with Argon. Further details about both this deposition protocol and the associated ALD reactor can be found elsewhere [35, 36].

2.4 Modification of PdNPs/CF with anti-OTA and BSA

A fresh stock solution of anti-OTA (1.0 µg mL^{-1}) was prepared in phosphate buffer saline solution (PBS) presenting a pH value of 7.4. The anti-OTA solution was mixed with 0.4 M EDC and 0.1 M NHS in the ratio of 4:1:1 and kept at 4.0 °C for 30 min, to activate the carboxyl groups in fragment crystallizable (Fc) region of anti-OTA [37]. Thereafter, the anti-OTA was ready for the two steps immobilization process onto the surface of PdNPs/CF. In a first step, 10 µL of anti-OTA with EDC-NHS was spread over the PdNPs/CF electrode and incubated at 4.0 °C for 6.0 h, after which it was washed with PBS to remove the unbounded or excess anti-OTA from the electrode surface. Secondly, 10 µL of BSA (0.1 %) was spread over anti-OTA/PdNPs/CF immunoelectrode surface, to block any non-specific active sites on the electrode (Scheme 1). The fabricated BSA/anti-OTA/PdNPs/CF immunoelectrode was kept at 4.0 °C when not in use.

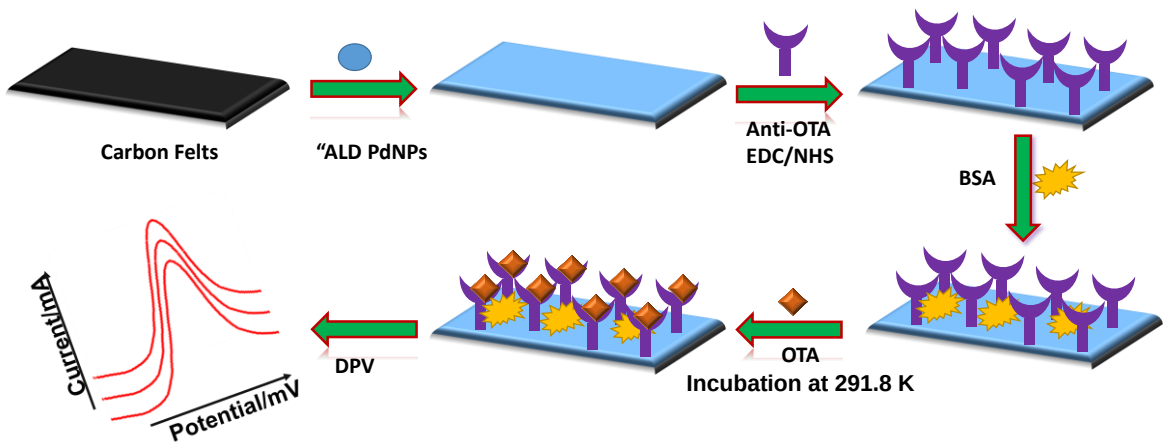

Scheme 1: Schematic representation of the preparation of BSA/anti-OTA/PdNPs/CF immunoelectrode.

2.5 Preparation of coffee samples

The stock solution of the coffee sample (1.0 mg mL^{-1}) was prepared by ultrasonicating a mixture of 10 mL of PBS and 10 mg of coffee for 2 h. Thereafter 1.0 mL of the prepared stock solution was spiked with different concentrations of OTA ranging from 0.5 to 20 ng mL^{-1}) and kept at 4.0 °C until further use.

2.6 Indirect detection of OTA

For the OTA measurements, 10 µL of OTA standards with different concentrations ranging from 0.5 to 20 ng mL^{-1} in PBS was pipetted onto the surface of the BSA/anti-OTA/PdNPs/CF immunoelectrodes and allowed to stand for 40 min at room temperature. DPV was used for the quantification of OTA and the measurements were conducted using a

5.0 mM $K_3Fe(CN)_6/K_4Fe(CN)_6$ (1:1) mixture in PBS (pH 7.0). The CVs were performed in 5.0 mM $K_3[Fe(CN)_6]$ supported by 1 M KCl in 0.1 M K_2HPO_4–KH_2PO_4 solution. The EIS measurement was performed in 1 M KCl containing equimolar $[Fe(CN)_6]^{3-/4-}$ with AC frequency from 0.1 to 10^5 Hz.

3. Results and Discussion

3.1. Physical and chemical characterizations of the electrodes

Surface morphology of the fabricated electrodes were characterized by SEM and TEM. Fig 1A shows the morphology of PdNPs deposited onto CF by ALD over 200 cycles resulting in the formation of uniformly dispersed NPs. The TEM images (Fig.S1 A, B & C) further revealed an average diameter of 6±2 nm for the PdNPs layer on the carbon substrate. It is clear from the SEM and the TEM images that the PdNPs were well-dispersed at the surface of the carbon substrate. These results were supported with X-Ray photoelectron microscopy to confirm the pure metallic form of Pd and inductively coupled plasma mass spectrometry (ICP-MS) to confirm the low metal loading limited at 0.85 wt.% (±0.1 %), corresponding to <0.1 mgPd cm^{-2} [35].

After immobilization of BSA onto anti-OTA/PdNPs/CF electrode, a smooth surface morphology was obtained as shown in Fig. 1B. The BSA was used to block non-binding sites of the anti-OTA/PdNPs/CF immunoelectrode. Further immobilization of OTA by incubation onto BSA/anti-OTA/PdNPs/CF results in a rough surface as can be seen in Fig.1C, which is indicative of optimum adsorption of OTA on the electrode surface.

The functional groups present in the fabricated immunosensor were investigated by ATR, with Fig. 1D showing the anti-OTA/PdNPs/CF (curve i) and BSA/anti-OTA/PdNPs/CF

(curve ii). A characteristic peak at 1671 cm^{-1} corresponding to -NH deformation in an amide-II bond, suggesting the covalent immobilization of anti-OTA on the electrode surface (curve i). The band seen around 1456 cm^{-1} is due to the vibration of $-CH_2$ aliphatic moiety of anti-OTA [37]. The band found at 852 cm^{-1} is due to free $-NH_2$ groups on the electrode surface. After BSA immobilization (curve ii; BSA/anti-OTA/PdNPs/CF), the band at 852 cm^{-1} completely disappeared, this confirms the blocking of nonspecific sites available on anti-OTA/PdNPs/CF immunoelectrode [38].

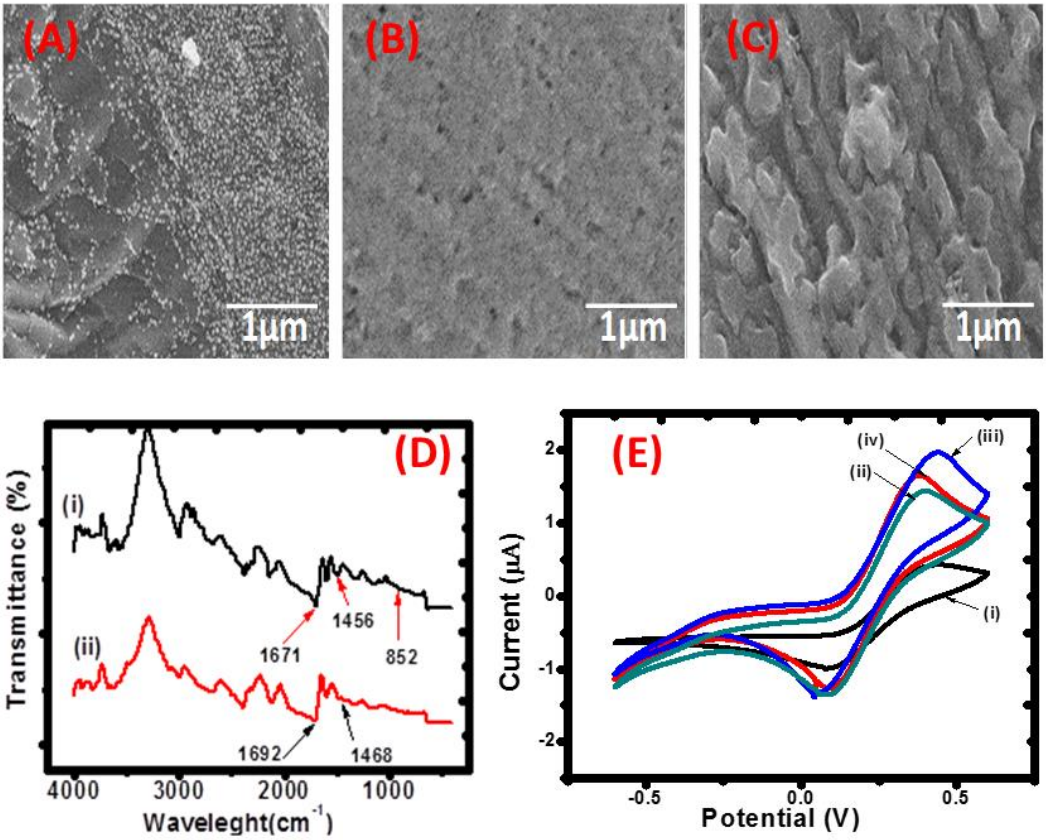

Fig.1. SEM images of PdNPs/CF electrode (A); BSA/anti-OTA/PdNPs/CF (B); and OTA/BSA/anti-OTA/PdNPs/CF (C) immunoelectrode. (D) ATR spectra of anti-OTA/PdNPs/CF (i); and BSA/ant-OTA/PdNPs/CF (ii) immunoelectrode; (E) CV comparison of CF electrode (i); PdNPs/CF (ii); anti-OTA/PdNPs/CF (iii) and BSA/anti-OTA/PdNPs/CF (iv) immunoelectrodes in PBS containing 5.0 mM $[Fe(CN)_6]^{3-/4-}$ solution.

The hydrophobic/hydrophilic nature of the modified electrode was investigated by measuring the water contact angle (CA) of the PdNPs/CF and BSA/anti-OTA/PdNPs/CF electrodes. The CA represents the level of wetting property on the solid-liquid interaction. A CA value of 56.2° for PdNPs electrode (Fig. S2A) indicates a reasonable hydrophilicity however, after immobilization of anti-OTA onto the PdNPs/CF electrode (Fig S2B) the CA value decreased to 14.3°, indicating that anti-OTA further enhanced the wettability properties of the electrode.

3.2. Electrochemical studies

3.2.1. Electrodes characterization through cyclic voltammetry (CV)

CV is one of the most convenient technique that is used to monitor the behavior of the modified electrode. Fig. 1 (E) shows the CV response obtained using 5.0 mM $[Fe(CN)_6]^{3-/4}$ in PBS for (i) CF (ii), PdNPs/CF (iii) anti-OTA/PdNPs/CF and (iv) BSA/anti-OTA/PdNPs/CF immunoelectrodes. A pair of well-defined redox peak was observed for the CF (curve i), This quasi-reversible redox peak was attributed to the transformation between $Fe(CN)_6^{4-}$ and $Fe(CN)_6^{3-}$. The low anodic peak current (Ipa) of 0.99 µA and 1.03 µA for the bare CF electrode and anti-OTA/CFE immunoelectrode demonstrates a poor electrochemical response of the CF electrode and hindrance of electron transfer caused by the insulation and steric hindrance produced by anti-OTA. On the other hand, the I_{pa} increased to 1.77 µA for the PdNPs/CF coated surface (curve ii). These results demonstrate that deposition of PdNPs onto the CF substrate accelerates the rate of electron transfer between analyte and working electrode, due to high surface area and improvement in catalytic activity of the electrode.

However, when anti-OTA were immobilized onto the PdNPs/CF electrode the I_{pa} increased to 2.05 µA (curve iii), indicating further enhanced sensitivity. This phenomenon is probably due to the fragmented crystalline (Fc) region of the anti-OTA and the amine groups that forms a penetrating path between anti-OTA and electrode [37]. The free site amino group of anti-OTA available onto immunoelectrode surface electrostatically interacts with redox species of electrolyte and facilitates the fast electron diffusion at the electrode. However, for the BSA/anti-OTA/PdNPs/CF electrode the I_{pa} decreased to 1.83 µA (curve iv), this is in agreement with the previous report stating that BSA inhibiting the diffusion of redox species towards the electrode [39]. Our results confirmed the successful fabrication of the BSA/anti-OTA/PdNPs/CF immunoelectrode.

3.2.2. Effects of scan rate

Cyclic voltammetry was used to study the interface kinetics of BSA/anti-OTA/PdNPs/CF immunoelectrode by varying scan rate from 10-100 mV/s as shown in Fig. S3A. The peak currents increase linearly with the increase of scan rates while there was a minor shift of peak potential towards more a positive potential and more faradic current is flowing on the electrode. This indicates that the electroactive species are confined at the electrode surface and the reaction of OTA is following an adsorption-controlled process [40].

3.2.3. Electrochemical impedance spectroscopy

Electrochemical impedance spectroscopy results are presented using a Nyquist plot of CF with different modification processes using $[Fe(CN)_6]^{3-/4-}$ as the electrolyte. EIS spectrum comprises of a semicircle and the linear part as illustrated in Figures 2A-B. The semicircle diameter represents the electron-transfer resistance (R_{ct}) and reveals the restricted diffusion of

the electrolyte through the multilayer system, directly related to the film permeability. A very small semicircle diameter is observed on anti-OTA/CF electrode Fig. S6A demonstrating a low charge transfer resistance for the electrochemical process. At low frequency, the linear part is associated with the mass transfer process. After the deposition of PdNPs on the CF, the capacitance increases. Fig. 2B (curve i) shows the modification with PdNPs increases the electrochemical active surface area. The amplification of electrochemical signal and the enhancement of the electron transfer rate of the sensor are due to the excellent electro-catalytic activity of PdNPs [41]. After immobilization of anti-OTA (curve ii) onto PdNPs/CF electrode, a remarkable decrease of the charge transfers resistance (R_{ct}) is observed. This phenomenon is attributed to the presence of positively charged amino residues on the antibody structure, which facilitates the electrochemical reaction [42]. The increased in electron transfer observed can also be attributed to the neutralization of surface negative charge upon reaction with EDC/Sulfo-NHS [43].

However, after immobilization of BSA (curve (iii)), both R_{ct} and the capacitance increased, due to the longer path for the electrons to move from the solution to the surface of the electrode. The EIS data in Fig. 2 (A and B) were further analyzed by fitting them to the simulation data using the equivalent circuit model shown in Fig. 2 (B) inset. The fitting parameters include the ohmic resistance of the electrolyte solution (R_s), C is the capacitance that arises due to coverage of the electrode surface with BSA, R_{ct} is a charge transfer resistance that is caused by the resistance of electrons between electrode and $Fe(CN)_6^{3-/4-}$ redox probe, R is electrolyte resistance in the pore and Q is the CPE arising due to CF surface and Warburg impedance (*W*). Yang and co-workers reported the similar equivalent circuit on their work, their equivalent fitting has, the interface ohmic resistance (R_d), double layer capacitances (CPE_{dl}) and pore adsorption capacitance (CPE_{ad}) [44]. Siddiqui also reported the

286 similar equivalent circuit that has the uncompensated resistance Rs, capacitance C, charge
287 transfer resistance Rct, R is electrolyte resistance in the pore and Q [45]. BSA layer makes the
288 electrode surface more homogenous and generates the capacitance of 0.4×10^{-8} F. Therefore,
289 BSA behaves as an insulator. Moreover, the ohmic resistance (Rs) of BSA/anti-
290 OTA/PdNPs/CF is estimated to be ~8.06 ohms, much lower than that of CF materials (~19.22
291 ohms) and PdNPs (~10.7 ohms).

292

293 **3.2.4. Effect of pH**

294 The pH is a key parameter when fabricating an immunosensor electrode, due to the strong
295 influence of the electrolyte on the electrochemical performance. This parameter was
296 investigated by monitoring the current response of immunoelectrodes in electrolytes in the
297 range of pH 6.0 - 8.0. In Fig. 2C the peak currents response increase from pH 6.0 to 7.0, then
298 gradually decreases beyond pH 7.0. This indicates that biomolecules on the electrode surface
299 can only provide optimum performance when they are on their original form at neutral pH as
300 the basic or acidic medium denatures them due to the interaction of H^+ or OH^- ion with amino
301 acid sequence of antibodies (anti-OTA) [39, 46]. The maximum value of the peak current was
302 observed at pH 7.0 and therefore it was selected as the optimum pH for the subsequent
303 experiments.

304

305 **3.2.5. Effect of incubation time**

306 The immunochemical reaction is the process whereby the antigen and antibody interacts
307 with each other to form the immunocomplex. Its formation depends on the interaction time
308 (incubation time) of the antibody and antigen. Therefore, in order to get the optimum value of

the incubation time, measurements of 1.0 ng mL^{-1} OTA on BSA/anti-OTA/PdNPs/CF imunoelectrode were recorded every 5 min for a duration of 60 min as shown in Fig. 2D. It was observed that the peak current rises with an increase in interaction time of the immunocomplex up to 40 min. Beyond 40 min, it remains constants due to the saturation of antibodies. Subsequently, duration of 40 min was selected as the optimum interaction time for the immunochemical interaction.

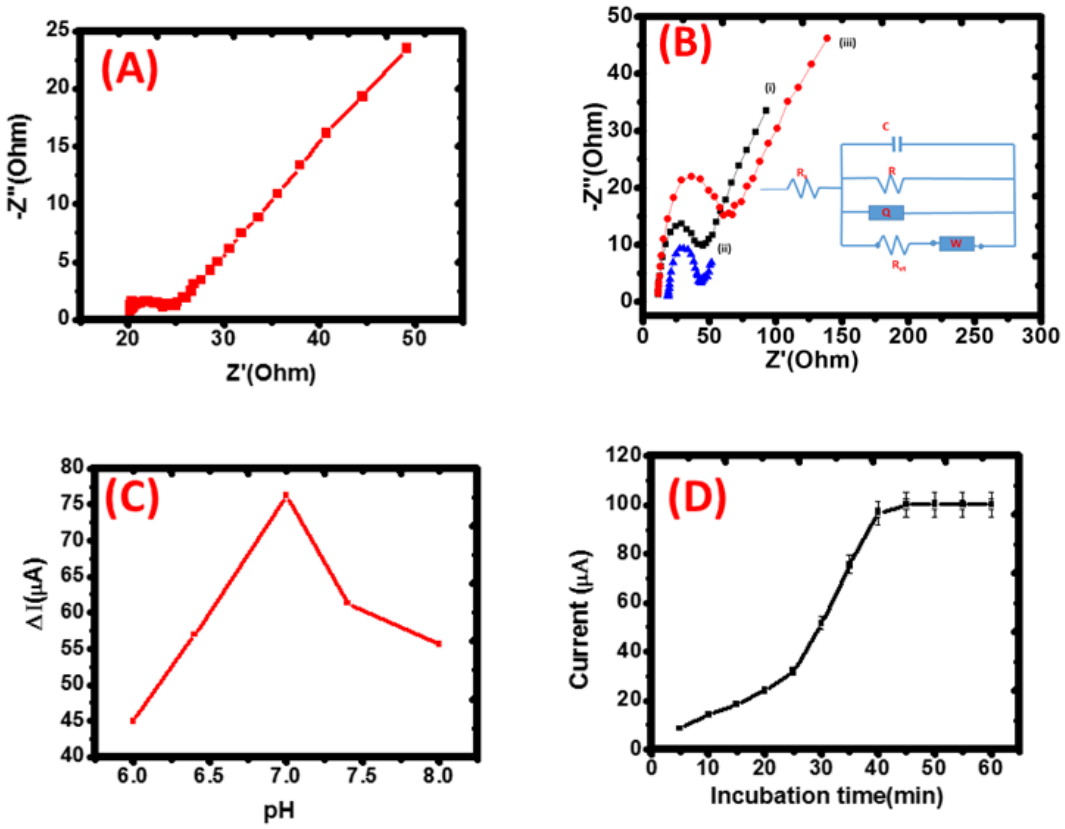

Fig. 2 (A) Nyquist plots of bare CF electrode; (B) PdNPs/CF (i); anti-OTA/PdNPs/CF (ii) and BSA/anti-OTA/PdNPs/CF (iii) modified electrode in PBS, pH 7.0., containing 5.0 mM $[Fe(CN)_6]^{4-/3-}$ solution: the inset shows the used equivalent circuit. (C) DPV response of BSA/anti-OTA/PdNPs/CF immunoelectrode of electrolyte pH and (D) incubation time.

3.2.6. Effects of anti-OTA concentration

The sensitivity of the immunosensor depends on the immunochemical reaction between the antigen and antibody (anti-OTA). The concentration of the antibody on the electrode surface is one of the most vital factors for the performance of the immunosensor. The effects of anti-OTA concentration on the immunoelectrode were investigated by immobilizing four different concentrations (0.5, 1, 5 and 10 μg mL^{-1}) of anti-OTA onto the PdNPs/CF electrode. The DPV responses of OTA were measured from 0.5 ng mL^{-1} to 2.5 ng mL^{-1}, in order to check the sensitivity of the fabricated immunoelectrodes. The change in current (denoted as ΔC), measured before and after immunoreaction, was calculated according to equation (1):

$$\Delta C = C_{anti\ OTA´OTA} - C_{anti\ OTA} \quad (1)$$

where $C_{anti\ OTA´OTA}$ is the value of the current after OTA coupling to the anti-OTA and $C_{anti\ OTA}$ represents the value of the current of the native immunosensor. The immunosensor with 1.0 μg mL^{-1} anti-OTA showed significant decrease in the current resulting in the LOD (0.25 ng mL^{-1}) and regression coefficient (R^2) of 0.9980 as shown in Fig. S3B and Table S1. However, the immunosensor with 5.0 μg mL^{-1} and 10 μg mL^{-1} anti-OTA concentrations showed a lower current with LODs and regression coefficients (R^2) of (0.39 ng mL^{-1}, 0.9850 and 0.44 ng mL^{-1} 0.9234 respectively. This is attributed to dense electrode surface with an inadequate binding between the antigen and antibody to cause a current change. Therefore, the thicker bioactive layer is the cause of a low performance of the immunosensor. Hence, 1.0 μg mL^{-1} anti-OTA was chosen as the optimal concentration for the further characterization of the immunosensor.

3.2.7. Sensing mechanisms of the immunosensor

In this work, the immunosensor was fabricated by covalently attaching antibody (Anti-OTA) to the PdNPs coated CF electrode surface. The PdNPs are employed as the carriers of the electrochemical capture probe to increase the change of peak currents. The ferricyanide solution is used as a redox mediator to generate the electron flow between bulk solution and working electrode as shown in Scheme 2. In the absence of OTA, the Anti-OTA offer a significantly strong Faradaic current. However, in the presence of OTA the faradic current decreases because, the formation of anti-OTA/OTA complex hinders the electron-transfer of $Fe(CN)_6^{3-}/Fe(CN)_6^{4-}$ [47, 48].

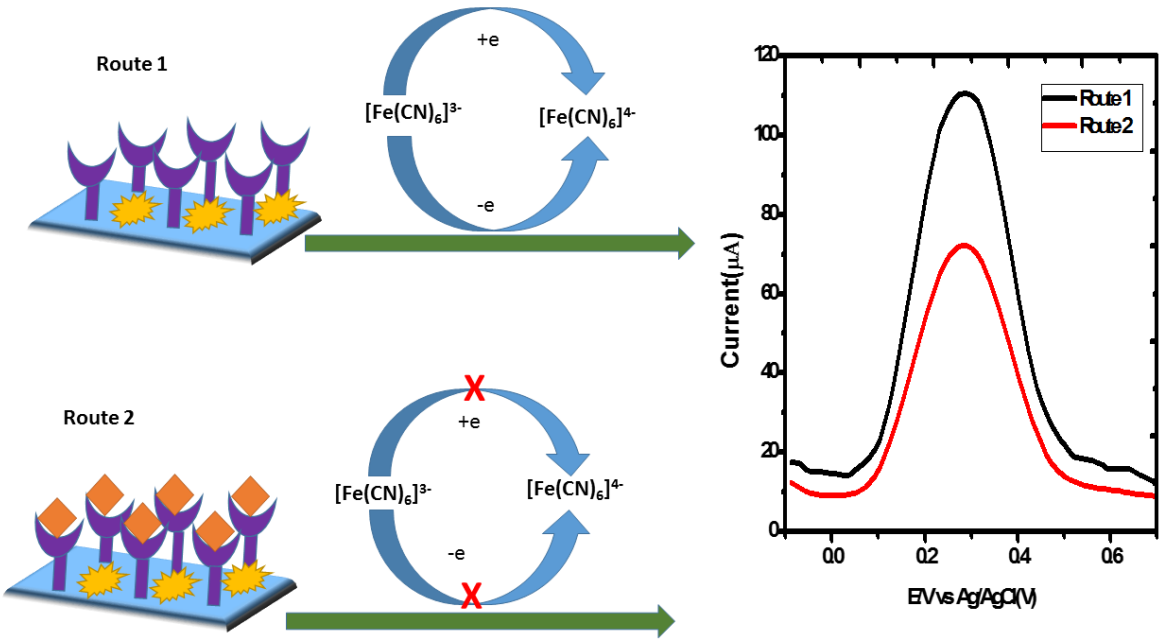

Scheme 2: The mechanism of the electrochemical immunosensor for the indirect detection of OTA.

3.2.8. Indirect quantification of OTA

The DPV response of BSA/anti-OTA/PdNPs/CF immunoelectrode recorded as a function of OTA concentration ranging from 0.5 to 20 ng mL^{-1} are depicted in Figure 3. The peak current (ΔI) decreased with an increase in OTA concentration, showing the formation of immunocomplex (antigen-antibody) at the electrode surface. This was established through the interaction of antigen with the antibody (anti-OTA) absorbed onto the BSA/anti-OTA/PdNPs/CF immunoelectrode which acts as an electron transporting layer [49, 50]. The resulting DPV measurements were then used to plot the calibration curve for OTA. The fabricated immunosensor BSA/anti-OTA/PdNPs/CF responds linearly to the logarithm concentration of OTA ranging from 0.5 to 20 ng mL^{-1} with LOD of 0.096 ng mL^{-1} (3×se)/m) and a regression coefficient (R^2) of 0.9960 [Fig. 3B].

The biosensing parameters of the fabricated immunosensor were then compared to the previously reported immunosensors for the detection of OTA (data given in Table S2). The fabricated BSA/anti-OTA/PdNPs/CF immunoelectrode have the ability to detect a very low concentration (96 pg mL^{-1}) of OTA as compared to other immunosensors [5, 8]. These results show that PdNPs/CF materials provide high surface affinity to bind antibodies.

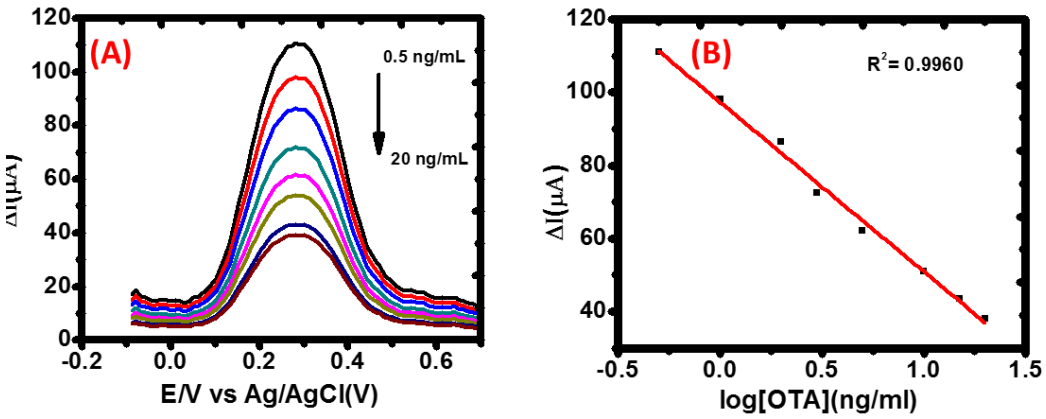

382

383 **Fig. 3.** (A) Electrochemical response studies of the BSA/anti-OTA/PdNPs/CF
384 immunoelectrode as a function of OTA using DPV (Conditions: Scan rate: 30 mV s^{-1},
385 Deposition time: 80 s, Pulse amplitude: 0.08 V and Pulse time: 0.03 s and (B) calibration
386 curve between the magnitude of current and OTA concentration.

387

388 **3.2.9. Recovery studies for the real samples**

389 In order to investigate the ability of the fabricated BSA/anti-OTA/PdNPs/CF
390 immunoelectrode, DPV responses were recorded in the presence of different concentrations of
391 the spiked coffee samples. Table 1 shows the outcomes of the recovery studies for spiked
392 sample in terms of electrochemical current. The DPV response was observed using five
393 concentrations (0.5, 1, 5, 10, 20 ng mL^{-1}), and the recovery was found in the range of 93.2-
394 98.9 % with proportional error ranging from 1.0 to 6.8 %. These measured values of RSD and
395 recovery were quite good and suggest that fabricated immunoelectrode is appropriate to be
396 applied to OTA detection.

397

Table 1: Determination of OTA concentration in spiked samples using BSA/anti-OTA/PdNPs/CF immunoelectrode

Spiked concentration (ng/mL)	DPV response for		Recovery (%)	Proportional error (%)
	Spiked sample (µA)	OTA (µA)		
0.5	98.45	100.56	97.9	2.1
1	95.70	96.70	98.9	1.0
5	58.78	63.10	93.2	6.9
10	42.40	43.60	97.3	2.8
20	36.89	38.15	96.7	3.3

3.2.10. Selectivity and shelf-life of immunoelectrode

Selectivity and shelf-life are also very important parameters of immunoelectrodes. The selectivity of the immunoelectrode was investigated by monitoring the DPV response of BSA/anti-OTA/PdNPs/CF in the presence of the interferences. Different interferences such as BSA, Aflatoxin B1 and L-Trytophan (10 ng mL^{-1}) were mixed with OTA (1 ng mL^{-1}), and the DVP response was assessed (Fig. S4B). There was no significant change in the DPV response after the interaction of the immunoelectrode with interfering compounds. This indicates that the fabricated immunoelectrode is only selective to OTA detection. The DPV technique was used to investigate the shelf-life of immunoelectrode on a regular interval of seven days up to three weeks using the optimized parameters. The fabricated immunoelectrode shown in Fig. S4A shows that is stable up to at least three weeks, with a slight change in current value (99.6 %) was observed. This suggests that BSA/anti-OTA/PdNPs/CF immunoelectrode is highly stable.

3.3. Reproducibility and repeatability of immunoelectrode

The reproducibility of the BSA/anti-OTA/PdNPs/CF immunoelectrode was studied using the interassay methods where DPV response was studied for six individual immunoelectrodes prepared independently as shown in Fig.S5A. The value of relative standard deviation (RSD) was found to be 5.6 %. Additionally, the repeatability of the immunoelectrode was investigated using one immunoelectrode for six successive measurements, and the results showed a good standard deviation of 1.4% as shown in Fig. S5B. The repeatability results show that the fabricated immunosensor can be reusable. In fact, the repeatability of the fabricated immunoensor shows that the standard deviation is below 2%, after six successive measurements conducted on one immunosensor. Further study would however be needed for a more precise understanding the reusability of the fabricated immunosensor.

Conclusion

In this study, we reported the fabrication and the characterization of a novel and highly efficient electrochemical immunosensor for the selective detection of OTA. Atomic layer deposition has been successfully used as an efficient route to produce highly dispersed PdNPs onto the surface of carbon felt (CF) electrodes, and the BSA and the anti-OTA antibodies were then grafted onto the composite structure via a carbodiimide cross linkage route. Subsequently, the developed immunosensor was used to detect the OTA in coffee samples. The fabricated BSA/anti-OTA/PdNPs/CF immunosensor showed outstanding electrochemical performances such as a wide detection range of 0.5-20 ng mL^{-1} and a LOD of 0.096 ng mL^{-1} towards the detection of OTA. This study also revealed that the PdNPs accelerate the electron

transfer rate on the large surface area electrodes. Additionally, the immobilization of anti-OTA on the surface of the electrodes offer specific intrinsic immuno-recognition, with an improved binding efficiency, wettability property and enhanced selectivity of the sensor. Finally, this study also revealed that the fabricated immunosensor were selective to OTA in the presence of interfering compounds and that the sensors were stable for up to three weeks. The results presented in this work open prospects for new sensing routes for molecules of interest in food products.

Acknowledgements

This work was financially supported by the French Embassy in South Africa through PhD scholarship, by the Council for Scientific and Industrial Research (CSIR, South Africa) and by the French National Agency (ANR, program MeNiNA - ANR-17-CE09-0049). The authors thank Bruno Navarra for technical support.

References

[1] J.C. Vidal, L. Bonel, A. Ezquerra, P. Duato, J.R. Castillo, An electrochemical immunosensor for ochratoxin A determination in wines based on a monoclonal antibody and paramagnetic microbeads, Analytical and bioanalytical chemistry, 403 (2012) 1585-1593.

[2] K.F. Nielsen, A.F. Ngemela, L.B. Jensen, L.S. De Medeiros, P.H. Rasmussen, UHPLC-MS/MS determination of ochratoxin A and fumonisins in coffee using QuEChERS extraction combined with mixed-mode SPE purification, Journal of agricultural and food chemistry, 63 (2015) 1029-1034.

[3] X. Liu, Z. Tang, Z. Duan, Z. He, M. Shu, X. Wang, S.J. Gee, B.D. Hammock, Y. Xu, Nanobody-based enzyme immunoassay for ochratoxin A in cereal with high resistance to matrix interference, Talanta, 164 (2017) 154-158.

[4] A. Karczmarczyk, K. Haupt, K.-H. Feller, Development of a QCM-D biosensor for Ochratoxin A detection in red wine, Talanta, 166 (2017) 193-197.

[5] P.K. Gupta, N. Pachauri, Z.H. Khan, P.R. Solanki, One pot synthesized zirconia nanoparticles embedded in amino functionalized amorphous carbon for electrochemical immunosensor, Journal of Electroanalytical Chemistry, 807 (2017) 59-69.

[6] A. Karczmarczyk, A.J. Baeumner, K.-H. Feller, Rapid and sensitive inhibition-based assay for the electrochemical detection of Ochratoxin A and Aflatoxin M1 in red wine and milk, Electrochimica Acta, 243 (2017) 82-89.

[7] A. Kaushik, P.R. Solanki, A.A. Ansari, S. Ahmad, B.D. Malhotra, Chitosan–iron oxide nanobiocomposite based immunosensor for ochratoxin-A, Electrochemistry Communications, 10 (2008) 1364-1368.

[8] F. Malvano, D. Albanese, R. Pilloton, M. Di Matteo, A highly sensitive impedimetric label free immunosensor for Ochratoxin measurement in cocoa beans, Food chemistry, 212 (2016) 688-694.

[9] E. Commission, Commission Regulation (EC) No 1881/2006 of 19 December 2006 setting maximum levels for certain contaminants in foodstuffs, Off J Eur Union, 364 (2006).

[10] A. Pittet, D. Royer, Rapid, low cost thin-layer chromatographic screening method for the detection of ochratoxin A in green coffee at a control level of 10 μg/kg, Journal of Agricultural and Food Chemistry, 50 (2002) 243-247.

[11] Y. Rodríguez-Carrasco, G. Font, J. Mañes, H. Berrada, Determination of mycotoxins in bee pollen by gas chromatography–tandem mass spectrometry, Journal of agricultural and food chemistry, 61 (2013) 1999-2005.

[12] S. Ahn, S. Lee, J. Lee, B. Kim, Accurate determination of ochratoxin A in Korean fermented soybean paste by isotope dilution-liquid chromatography tandem mass spectrometry, Food chemistry, 190 (2016) 368-373.

[13] R. Viter, M. Savchuk, I. Iatsunskyi, Z. Pietralik, N. Starodub, N. Shpyrka, A. Ramanaviciene, A. Ramanavicius, Analytical, thermodynamical and kinetic characteristics of photoluminescence immunosensor for the determination of Ochratoxin A, Biosensors and Bioelectronics, 99 (2018) 237-243.

[14] V. Myndrul, R. Viter, M. Savchuk, N. Shpyrka, D. Erts, D. Jevdokimovs, V. Silamiķelis, V. Smyntyna, A. Ramanavicius, I. Iatsunskyi, Porous silicon based photoluminescence immunosensor for rapid and highly-sensitive detection of Ochratoxin A, Biosensors and Bioelectronics, 102 (2018) 661-667.

[15] Z. Sun, X. Wang, Z. Tang, Q. Chen, X. Liu, Development of a biotin-streptavidin-amplified nanobody-based ELISA for ochratoxin A in cereal, Ecotoxicology and environmental safety, 171 (2019) 382-388.

[16] A.L. Manizan, M. Oplatowska-Stachowiak, I. Piro-Metayer, K. Campbell, R. Koffi-Nevry, C. Elliott, D. Akaki, D. Montet, C. Brabet, Multi-mycotoxin determination in rice, maize and peanut products most consumed in côte d'ivoire by uhplc-ms/ms, Food control, 87 (2018) 22-30.
[17] M.A. Andrade, F.M. Lanças, Determination of Ochratoxin A in wine by packed in-tube solid phase microextraction followed by high performance liquid chromatography coupled to tandem mass spectrometry, Journal of Chromatography A, 1493 (2017) 41-48.
[18] M.L. Savastano, I. Losito, S. Pati, Rapid and automatable determination of ochratoxin A in wine based on microextraction by packed sorbent followed by HPLC-FLD, Food Control, 68 (2016) 391-398.
[19] J. Zhang, Y.-K. Xia, M. Chen, D.-Z. Wu, S.-X. Cai, M.-M. Liu, W.-H. He, J.-H. Chen, A fluorescent aptasensor based on DNA-scaffolded silver nanoclusters coupling with Zn (II)-ion signal-enhancement for simultaneous detection of OTA and AFB1, Sensors and Actuators B: Chemical, 235 (2016) 79-85.
[20] E.-J. Jo, H. Mun, S.-J. Kim, W.-B. Shim, M.-G. Kim, Detection of ochratoxin A (OTA) in coffee using chemiluminescence resonance energy transfer (CRET) aptasensor, Food chemistry, 194 (2016) 1102-1107.
[21] M. Heurich, M.K.A. Kadir, I.E. Tothill, An electrochemical sensor based on carboxymethylated dextran modified gold surface for ochratoxin A analysis, Sensors and Actuators B: Chemical, 156 (2011) 162-168.
[22] H. Zejli, K.Y. Goud, J.L. Marty, Label free aptasensor for ochratoxin A detection using polythiophene-3-carboxylic acid, Talanta, 185 (2018) 513-519.
[23] N. Liu, D. Nie, Y. Tan, Z. Zhao, Y. Liao, H. Wang, C. Sun, A. Wu, An ultrasensitive amperometric immunosensor for zearalenones based on oriented antibody immobilization on a glassy carbon electrode modified with MWCNTs and AuPt nanoparticles, Microchimica Acta, 184 (2017) 147-153.
[24] L. Rivas, C.C. Mayorga-Martinez, D. Quesada-González, A. Zamora-Gálvez, A. de la Escosura-Muñiz, A. Merkoçi, Label-free impedimetric aptasensor for ochratoxin-A detection using iridium oxide nanoparticles, Analytical chemistry, 87 (2015) 5167-5172.
[25] L. Bonel, J.C. Vidal, P. Duato, J.R. Castillo, Ochratoxin A nanostructured electrochemical immunosensors based on polyclonal antibodies and gold nanoparticles coupled to the antigen, Analytical Methods, 2 (2010) 335-341.
[26] S.M. Taghdisi, N.M. Danesh, H.R. Beheshti, M. Ramezani, K. Abnous, A novel fluorescent aptasensor based on gold and silica nanoparticles for the ultrasensitive detection of ochratoxin A, Nanoscale, 8 (2016) 3439-3446.
[27] V. Solano-Umaña, J. Vega-Baudrit, Gold and silver nanotechnology on medicine, Journal of Chemistry and Biochemistry, 3 (2015) 21-33.
[28] A. Tiwari, M. Ramalingam, H. Kobayashi, A.P. Turner, Biomedical materials and diagnostic devices, John Wiley & Sons2012.
[29] C. Zhang, J. Tang, L. Huang, Y. Li, D. Tang, In-situ amplified voltammetric immunoassay for ochratoxin A by coupling a platinum nanocatalyst based enhancement to a redox cycling process promoted by an enzyme mimic Microchimica Acta, 184 (2017) 2445-2453.
[30] M. Weber, M. Verheijen, A. Bol, W. Kessels, Sub-nanometer dimensions control of core/shell nanoparticles prepared by atomic layer deposition, Nanotechnology, 26 (2015) 094002.
[31] S.M. George, Atomic layer deposition: an overview, Chemical reviews, 110 (2009) 111-131.

[32] I.J. Raaijmakers, Current and future applications of ALD in micro-electronics, ECS Transactions, 41 (2011) 3-17.
[33] A.J. Mackus, M.J. Weber, N.F. Thissen, D. Garcia-Alonso, R.H. Vervuurt, S. Assali, A.A. Bol, M.A. Verheijen, W.M. Kessels, Atomic layer deposition of Pd and Pt nanoparticles for catalysis: on the mechanisms of nanoparticle formation, Nanotechnology, 27 (2015) 034001.
[34] M. Weber, A. Julbe, A. Ayral, P. Miele, M. Bechelany, Atomic layer deposition for membranes: Basics, challenges, and opportunities, Chemistry of Materials, 30 (2018) 7368-7390.
[35] O. Graniel, M. Weber, S. Balme, P. Miele, M. Bechelany, Atomic layer deposition for biosensing applications, Biosensors and Bioelectronics, (2018).
[36] M. Weber, J.-Y. Kim, J.-H. Lee, J.-H. Kim, I. Iatsunskyi, E. Coy, P. Miele, M. Bechelany, S.S. Kim, Highly Efficient Hydrogen Sensors Based on Pd Nanoparticles Supported on Boron Nitride Coated ZnO Nanowires, Journal of Materials Chemistry A, (2019).
[37] P.K. Gupta, S. Tiwari, Z.H. Khan, P.R. Solanki, Amino acid functionalized ZrO 2 nanoparticles decorated reduced graphene oxide based immunosensor, Journal of Materials Chemistry B, 5 (2017) 2019-2033.
[38] P.R. Solanki, M.K. Patel, M.A. Ali, B. Malhotra, A chitosan modified nickel oxide platform for biosensing applications, Journal of Materials Chemistry B, 3 (2015) 6698-6708.
[39] M.A. Ali, K. Kamil Reza, S. Srivastava, V.V. Agrawal, R. John, B.D. Malhotra, Lipid–lipid interactions in aminated reduced graphene oxide interface for biosensing application, Langmuir, 30 (2014) 4192-4201.
[40] Y. Xiang, M.B. Camarada, Y. Wen, H. Wu, J. Chen, M. Li, X. Liao, Simple voltammetric analyses of ochratoxin A in food samples using highly-stable and anti-fouling black phosphorene nanosensor, Electrochimica Acta, 282 (2018) 490-498.
[41] G. Zhang, Z. Liu, L. Fan, Y. Guo, Electrochemical prostate specific antigen aptasensor based on hemin functionalized graphene-conjugated palladium nanocomposites, Microchimica Acta, 185 (2018) 159.
[42] A.-E. Radi, X. Munoz-Berbel, V. Lates, J.-L. Marty, Label-free impedimetric immunosensor for sensitive detection of ochratoxin A, Biosensors and Bioelectronics, 24 (2009) 1888-1892.
[43] F. Conzuelo, M. Gamella, S. Campuzano, D.G. Pinacho, A.J. Reviejo, M.P. Marco, J.M. Pingarrón, Disposable and integrated amperometric immunosensor for direct determination of sulfonamide antibiotics in milk, Biosensors and Bioelectronics, 36 (2012) 81-88.
[44] G. Yang, D. Chen, P. Lv, X. Kong, Y. Sun, Z. Wang, Z. Yuan, H. Liu, J. Yang, Core-shell Au-Pd nanoparticles as cathode catalysts for microbial fuel cell applications, Scientific reports, 6 (2016) 35252.
[45] S. Siddiqui, Z. Dai, C.J. Stavis, H. Zeng, N. Moldovan, R.J. Hamers, J.A. Carlisle, P.U. Arumugam, A quantitative study of detection mechanism of a label-free impedance biosensor using ultrananocrystalline diamond microelectrode array, Biosensors and Bioelectronics, 35 (2012) 284-290.
[46] C. Zhou, D. Liu, L. Xu, Q. Li, J. Song, S. Xu, R. Xing, H. Song, A sensitive label–free amperometric immunosensor for alpha-fetoprotein based on gold nanorods with different aspect ratio, Scientific reports, 5 (2015) 9939.
[47] Y.S. Kim, J.H. Niazi, M.B. Gu, Specific detection of oxytetracycline using DNA aptamer-immobilized interdigitated array electrode chip, Analytica Chimica Acta, 634 (2009) 250-254.

612 [48] L. Zhou, D.-J. Li, L. Gai, J.-P. Wang, Y.-B. Li, Electrochemical aptasensor for the
613 detection of tetracycline with multi-walled carbon nanotubes amplification, Sensors and
614 Actuators B: chemical, 162 (2012) 201-208.
615 [49] A. Kaushik, P.R. Solanki, A.A. Ansari, S. Ahmad, B.D. Malhotra, A nanostructured
616 cerium oxide film-based immunosensor for mycotoxin detection, Nanotechnology, 20 (2009)
617 055105.
618 [50] Q. Li, L. Zeng, J. Wang, D. Tang, B. Liu, G. Chen, M. Wei, Magnetic mesoporous
619 organic− inorganic NiCo2O4 hybrid nanomaterials for electrochemical immunosensors, ACS
620 applied materials & interfaces, 3 (2011) 1366-1373.

621